JE Noll, J Jeffery, F Al-Ejeh, R Kumar, KK Khanna, DF Callen and PM Neilsen
Mutant p53 drives multinucleation and invasion through a process that is suppressed by ANKRD11
Oncogene, 2012; 2(12):1203-1217

Final publication at http://dx.doi.org/10.1038/onc.2011.456

Mutant p53 drives multinucleation and invasion through a process that is suppressed by ANKRD11

Jacqueline E. Noll[1,*], Jessie Jeffery[2], Fares Al-Ejeh[2], Raman Kumar[1], Kum Kum Khanna[2], David F. Callen[1] and Paul M. Neilsen[1,3]

[1] Cancer Therapeutics Laboratory, Discipline of Medicine, University of Adelaide, Frome Rd, Adelaide, South Australia, Australia

[2] Signal Transduction Laboratory, Queensland Institute of Medical Research, Brisbane, Queensland, Australia

[3] Sarcoma Research Group, Discipline of Medicine, University of Adelaide & Hanson Institute, Frome Rd, Adelaide, South Australia, Australia

[*] Corresponding author: Jacqueline Noll

email: jacqueline.noll@adelaide.edu.au

Phone: (618) 82223450

Running Title: ANKRD11 suppresses mutant p53 gain-of-function

Word Count: 5037

Abstract

Mutations of p53 in cancer can result in a gain-of-function (GOF) associated with tumour progression and metastasis. We show that inducible expression of several p53 "hotspot" mutants promote a range of centrosome abnormalities including centrosome amplification, increased centrosome size and loss of cohesion, which lead to mitotic defects and multinucleation. These mutant p53 expressing cells also exhibit a change in morphology and enhanced invasive capabilities. Consequently, we sought for a means to specifically target the function of mutant p53 in cancer cells. This study has identified ANKRD11 as a key regulator of the oncogenic potential of mutant p53. Loss of expression of ANKRD11 with p53 mutation defines breast cancer patients with poor prognosis. ANKRD11 alleviates the mitotic defects driven by mutant p53 and suppresses mutant p53-mediated mesenchymal-like transformation and invasion. Mechanistically, we show that ANKRD11 restores a native conformation to the mutant p53 protein and causes dissociation of the mutant p53•p63 complex. This represents the first evidence of an endogenous protein with the capacity to suppress oncogenic properties of mutant p53.

Keywords: ANKRD11 / Centrosome aberrations / Gain of function / Invasion / Mutant p53

Introduction

The p53 protein is a tumour suppressor that predominantly functions as a sequence-specific transcription factor regulating the expression of various target genes involved in cell-cycle arrest, apoptosis, senescence, DNA repair, and inhibition of angiogenesis and metastasis, in response to a variety of cellular insults (Lane 1992, Liu and Chen 2006). Approximately 50% of all human cancers contain a mutation in the *TP53* gene (Hollstein et al 1991, Vogelstein et al 2000) with the majority of these mutations occurring within the DNA-binding domain (DBD) (Bullock and Fersht 2001, Olivier et al 2010). Mutations at six specific residues in the DBD have been identified as mutational "hotspots" and are classified into two categories: DNA contact mutants (R248Q, R248W, R273C and R273H) involving residues which specifically interact with DNA, and structural mutants (R175H, G245S, R249S and R282W) which exhibit local or global distortions of the p53 protein structure (Cho et al 1994).

Mutant p53 proteins exhibit both loss- and gain-of-function characteristics. Loss-of-function is largely due to the inability of mutant p53 to bind the canonical wild-type p53 binding site, resulting in an inability to transactivate its target genes (Kato et al 2003, Scian et al 2004), an attenuated tumour suppressive function and consequently, deregulated cellular growth and apoptosis. In contrast, gain-of-function (GOF) characteristics of mutant p53 are critical for tumour progression and metastasis (Brosh and Rotter 2009, Oren and Rotter 2010). A variety of GOF phenotypes of mutant p53 have been reported including increased invasive and metastatic potential of cells, resistance to chemotherapies, regulation of pro-inflammatory and anti-

apoptotic pathways and increased genomic instability (Oren and Rotter 2010), all of which give mutant p53 expressing cells a selective growth and survival advantage.

Various strategies have been developed to target mutant p53 in cancers including small molecules that aim to restore the native conformation to the unfolded mutant p53 proteins (Bykov et al 2002), or target their interactions with family members (Di Agostino et al 2008, Kravchenko et al 2008). Using a novel protein-based approach, we have previously shown that ANKRD11 can restore normal transactivation potential to a p53 hotspot mutant in a breast cancer cell line (Neilsen et al 2008), and represents the first endogenously-expressed protein with a capacity to rescue mutant p53 function. In this study we utilised a panel of ecdysone-inducible cell lines in a p53 null background to express various p53 hotspot mutants to investigate cellular processes that are driven by mutant p53 GOF and which can be suppressed by ANKRD11.

RESULTS

p53 mutation and loss of ANKRD11 expression define cancer patients with poor prognosis

Previously, we established that ANKRD11 could restore normal transactivation potential to the p53-R273H mutant (Neilsen et al 2008) and thus we explored a wider role for ANKRD11 in the suppression of the oncogenic functions of mutant p53. ANKRD11 was robustly expressed in the normal breast epithelium, however was down-regulated in the majority of breast tumours (Fig. 1A). Analysis of the expression profiling of a cohort of breast tumours (Miller et al 2005) revealed that the combination of p53 mutation and loss of ANKRD11 expression defined a subset of patients with poor outcomes (Fig. 1B). Low ANKRD11 expression was also significantly associated with poor survival in cohorts of bladder and lung tumours (Supp. Fig. S1). Furthermore, loss of ANKRD11 expression was significantly associated with invasion to the lymph nodes in breast tumours expressing mutant p53 (Fig. 1C). Collectively, the data support a role for ANKRD11 as a suppressor of the oncogenic potential of mutant p53. We subsequently sought to understand the mechanism of this suppression.

Mutant p53 drives centrosome abnormalities and multinucleation that can be suppressed by ANKRD11

Several biological pathways were examined to assess mutant p53 GOF. These assays were based on the inducible expression of mutant p53 in the H1299 p53-null genetic background. In these cell lines, p53 can be expressed dose-dependent to the inducing agent, Ponasterone A (PonA). Furthermore, the inducible expression of wild-type p53 was equivalent to DNA damage induced activation of the p53 pathway,

and mutant p53 levels comparable to endogenous mutant p53 expression in cancer cell lines (Supp. Fig. S2).

Induction of mutant p53 in H1299 cells resulted in a time-dependent increase in multinucleation, with approximately 25% of cells exhibiting more than one nuclei following 96 hours of mutant p53 expression (Fig. 2A). Giant multinucleated H1299 cells were observed following prolonged expression of mutant p53 (Supp. Fig. S3A). Co-staining cells for α-tubulin and γ-tubulin, markers for microtubules and centrosomes respectively, showed induction of mutant p53 was associated with a small but significant increase in the number of centrosomes per cell (Fig 2B). The limited size of the increase was most likely due to the small number of cell cycles observed. Centrin immunofluorescence studies demonstrated that these aberrant centrosomal frequencies were not due to centriole splitting (Supp. Fig. S3B). However, there was a significant increase in average centrosome size (Fig. 2C), which was not due to increased γ-tubulin expression (Supp. Fig. S3B) A significant increase in the average distance between centrosomes was also observed (Fig. 2D). These observations are demonstrated as *bone fide* mutant p53 GOF pathways as multinucleation and centrosomal aberrations were not observed in cells with induced wild-type p53 (Fig. 2A-D), and importantly multinucleation of EI-H1299 cells was not observed following treatment with PonA (Supp. Fig. S4). Furthermore, at 24 hours post-induction cells were observed with centrosomal amplification without multinucleation, suggesting that the defects in centrosomal duplication are driving the multinucleation phenotype and not mitotic failure.

To examine how the restored expression of ANKRD11 would impact upon the ability of mutant p53 to disrupt normal mitotic fidelity, ANKRD11 was stably-expressed in EI p53 mutant cells (which exhibit undetectable ANKRD11 expression) to approximate physiological levels, as judged by the levels observed in primary epithelial cells (Supp. Fig. S5). Restoring ANKRD11 expression completely abolished the ability of induced p53-R175H to drive multinucleation in EI p53-R175H cells (Fig. 2A). A similar result was also seen following induction of p53-R248W in the presence of ANKRD11 expression (Supp. Fig. S6). Furthermore, induction of p53-R175H failed to modulate centrosome size, separation or cohesion in the presence of restored ANKRD11 expression (Fig. 2B-D). Importantly, ANKRD11 did not influence p53-R175H mutant protein levels following exposure to the inducing agent, PonA (Fig. 2E). Together these findings illustrate the capacity of ANKRD11 to suppress the oncogenic potential of a p53 GOF mutant.

Mutant p53 expression is associated with chromosome segregation defects that can be suppressed by ANKRD11

As centrosome abnormalities have previously been linked to aberrant mitotic progression (Mailand et al 2002, Wonsey and Follettie 2005), we next examined the mutant p53 expressing cells ability to undergo mitosis. The defects in centrosome duplication and segregation in the induced mutant p53 cells was associated with a 20 to 30% increase in the frequency of abnormal mitotic spindles (Fig. 3A & B), and a significant increase in cells with lagging chromosomes (Fig. 3C) and anaphase bridges (Fig. 3D) compared with uninduced cells. The duration of mitosis, as assessed by live cell imaging, showed mutant p53 cells slowed the progression through mitosis to 72-75 mins (p<0.03) compared with 57-58 minutes in uninduced H1299 cells (Fig.

3E, Movies S1-S6). These findings show that mutant p53 expression does impact upon the normal execution of mitosis.

In the presence of restored ANKRD11 expression, the ability of induced p53-R175H to drive the formation of abnormal spindles, lagging chromosomes and anaphase bridges was completely ablated (Fig. 3A-D). Furthermore, the induced EI p53-R175H cells expressing ANKRD11 exhibited an average of 60 minutes in mitosis as compared to 75 minutes for induced p53-R175H alone (Fig. 3E, Movies S7-S8). These observations indicate that p53 mutants cannot drive tumourigenesis in the presence of physiological levels of ANKRD11.

Mutant p53 induces a mesenchymal morphology that is suppressed by ANKRD11

Gene expression arrays were used to determine the specific genes and pathways regulated upon induction of the p53-R175H mutant (Table 1). Following analysis of microarray expression data, Ingenuity Pathway Analysis revealed that many of the genes regulated by p53-R175H were shared across multiple biological pathways, which converged towards a network involved in cell motility and cell-to-cell signaling/interaction (Table 1, Supp. Fig. S7). Consequently, we investigated if induction of mutant p53 affected colony formation and morphology of epithelial H1299 cells. Control H1299 cells grew from single cells as tight colonies with defined boundaries, typical of epithelial cells (Fig. 4A, left). Upon induction of a structural (R175H) or DNA contact (R248Q) mutant, cells acquired an elongated mesenchymal-like morphology and exhibited disordered growth and decreased colony density (Fig. 4A, middle). In addition, ZO-1 immunofluorescence of EI p53-R175H cells showed

that cells dissociated from each other within 16 hours of p53-R175H induction (Fig. 4B), which is indicative of an invasive phenotype.

As we had already shown that ANKRD11 could alleviate the mitotic defects caused by mutant p53 induction, we next aimed to determine if the mesenchymal-like morphology of mutant p53-expressing cells could also be suppressed by ANKRD11. Physiological ANKRD11 expression in EI p53-R175H cells suppressed the mesenchymal-like phenotype, as demonstrated by a retention of tight colony formation following p53-R175H induction (Fig. 4A, right & Fig. 4B). Stable ANKRD11 expression in EI p53-R248Q cells also resulted in a restoration of the epithelial-like phenotype (Fig. 4A, right).

ANKRD11 suppresses mutant p53 invasive GOF

Mutant p53 GOF plays a key role in tumour progression, particularly through migration, invasion and metastasis. As induction of p53-R175H gave rise to an invasive phenotype, we aimed to determine if this was associated with an increased invasive capacity. The ability of uninduced or induced cells to invade through matrigel toward a chemo-attractant was measured in real-time using the Xcelligence system. Induction of p53-R175H did indeed result in an enhanced invasive capacity of H1299 cells, as demonstrated by a 2.5-fold ($p<0.05$) increased rate of invasion (Fig. 5). Stable expression of ANKRD11 in this system also ablated the ability of the induced R175H mutant to drive invasion (Fig. 5). Importantly, we also demonstrate that ANKRD11 can influence the tumorigenic properties of an additional mutant p53-expressing cancer cell line, MDA-MB-468 (p53 R273H). Expression of ANKRD11 in

this cell line was shown to slow the rate of migration of the MDA-MB-468 breast cancer cell line in a mutant p53-dependent manner (Supp. Fig. S8).

ANKRD11 restores a wild-type conformation and function to the p53-R175H mutant protein

We speculate that ANKRD11 can restore normal p53 function to p53 mutants as a consequence of its ability to directly interact with the mutant p53 proteins and revert the protein to a wild-type p53 conformation. We have previously shown the ankyrin repeat domain (ANKRD11$^{144\text{-}288aa}$) to directly interact with wild-type p53 (Neilsen et al 2008). We confirmed through co-immunoprecipitation assays that ANKRD11$^{144\text{-}288aa}$ could interact with both wild-type and eight p53 hotspot mutants (Fig. 6A). Further to these findings, we identified the C-terminus of p53 (p53$^{325\text{-}393aa}$) as the minimal region required for interaction with the ankyrin domain of ANKRD11 (Supp. Fig. S9).

To test the ability of ANKRD11 to affect mutant p53 tertiary structure, we utilised the conformation specific p53 antibody PAb1620 which recognises the wild-type p53 native protein structure under non-denaturing conditions (Milner et al 1987). In the presence of ANKRD11, induced p53-R175H exhibited an enhanced binding to the PAb1620 antibody, in comparison to that observed in the absence of ANKRD11 (Fig. 6B). These data suggest the association of ANKRD11 with p53-R175H restores the mutant protein conformation to more closely resemble the wild-type protein, thus facilitating recognition by the PAb1620 antibody. This newly adopted 'wild-type' conformation of the mutant p53 protein was also associated with restoration of p53 target gene expression by the p53 mutant to a level similar to that achievable by wild-

type p53 (Supp. Fig. S10). This restoration of transcriptional activity to the mutant p53 protein is also accompanied by a reduction in the percentage of cells undergoing mitosis, as demonstrated by MPM2 staining. Induction of wild-type p53 leads to a 65% reduction in cells undergoing mitosis ($p<0.01$) which is not seen following induction of various mutant p53 proteins. However, in the presence of ANKRD11, induction of the p53-R175H mutant leads to a significant ($p<0.01$) reduction in cells in mitosis (Supp. Fig. S11).

ANKRD11 impedes mutant p53-p63 and mutant p53-p73 complex formation

Previous studies have established that wild-type p53 does not interact with p63 and p73 while p53 mutants, including R175H, R249S and R273H exhibit GOF interactions with p63 and p73 (Gaiddon et al 2001, Strano et al 2000, Strano et al 2002). Immunoprecipitation in H1299 cells of co-transfected TAp63 and p53 mutants, including the eight p53 hotspot mutants, encompassing both DNA contact (R248Q, R248W, R273C and R273H) and structural (R175H, G245S, R249S, R282W) mutants suggest that p63 was primarily sequestered by p53 structural mutants (Fig. 7A). The DNA contact mutant p53-R273H also weakly co-precipitated with p63, which is consistent with previously published reports, while the remaining three DNA contact mutants did not interact (Fig. 7A). The same subset of p53 mutants that interacted with p63 were also shown to form a complex with TAp73 (Fig. 7B). Since the interaction between mutant p53 and p63 contributes to the invasive GOF of mutant p53 in H1299 cells (Muller et al 2009) we speculated that the suppressive functions of ANKRD11 are due, in part, to an interference with mutant p53•p63 complex formation.

Immunoprecipitation results demonstrated the formation of an R175H•p63 complex in the absence of ANKRD11 (Fig. 7C, lane 7). However, expression of the complete ankyrin domain (ANKRD11$^{144\text{-}288aa}$) resulted in dissociation of the R175H•p63 complex by up to 62 % (Fig. 7C, lane 8). ANKRD11$^{144\text{-}288aa}$ was also co-expressed with p53-R175H and p73 in the same system, and the interaction between R175H and p73 was reduced to 56% of the base-line (Fig. 7D). These results indicate that the association of ANKRD11 with mutant p53 disrupts its ability to interact with both p63 and p73. Further immunoprecipitation experiments with various regions encompassing the five ankyrin repeats present in ANKRD11 enabled the region of the domain that disrupts the mutant p53•p63 interaction to be defined. Ankyrin repeats one to three dissociated the p53-R175H•p63 complex by approximately 54% (Fig. 7C, lane 9). The R175H•p63 interaction was, however, maintained in the presence of ankyrin repeats four and five (Fig. 7C, lane 10). Expression of the first ankyrin repeat did not dissociate the R175H•p63 complex, however expression of repeats two and three resulted in a 21% decrease in the observed interaction between p53-R175H and p63 (Supp. Fig. S12). It was therefore inferred that an 80 amino acid region of ANKRD11 (ANKRD11$^{144\text{-}288aa}$) dissociated the R175H•p63 complex, with a slight reduction in complex formation also observed following co-expression of a 50 amino acid region (ANKRD11$^{176\text{-}225aa}$). These results are summarised in Figure 7E.

Discussion

Our current understanding of the GOF properties of mutant p53 is largely based on studies involving stable expression of p53 mutants in a p53 null background (Dong et al 2009, Muller et al 2009) or mutant p53 knock-in transgenic animal models (Song et al 2007). These systems have proven useful to functionally characterise the persistent, long-term oncogenic properties of mutant p53 such as invasion, metastasis and large-scale genetic abnormalities. However, using the ecdysone-inducible system, we have been able to directly investigate the primary pathways that are initiated by mutant p53 expression and which ultimately lead to its GOF, as well as identify ANKRD11 as an endogenously expressed protein capable of suppressing mutant p53 GOF.

Knockdown of endogenous mutant p53 in MDA-MB-468 cells results in reduced metastasis in a mouse model (Adorno et al 2009). Expression of ANKRD11 in MDA-MB-468 cells also significantly reduced their ability to form colonies on plastic (Neilsen et al 2008). Furthermore, loss of ANKRD11 expression with p53 mutation defines breast cancer patients with invasive tumours and poor prognosis (Fig. 1). Low ANKRD11 expression is also correlated with poor 5-year survival in bladder and lung cancer patients (Supp. Fig. S1). Loss-of-heterozygosity of chromosome 16q24 (the genomic location of the *ANKRD11* gene) is associated with good prognosis in breast cancer patients (Hansen et al 1998), therefore the observation that survival is higher in the wild-type p53 expressing breast tumours with low ANKRD11 expression may be an artefact of the loss of the 16q genomic region and not specific to ANKRD11. The correlation of low ANKRD11 expression and poor survival in mutant p53 expressing breast tumours support a role for

ANKRD11 as a suppressor of the oncogenic potential of mutant p53. Using the ecdysone-inducible system, we established three biological assays for investigating mutant p53 GOF and the effect of ANKRD11 on these processes. Specifically we investigated mitotic defects arising from centrosome abnormalities, cellular morphology changes and invasion.

Taking this approach, we show inducible expression of three p53 'hotspot' mutants result in multinucleation, centrosome aberrations, and a significant increase in the percentage of cells with abnormal spindles (Fig. 2 & 3). Previous studies link aberrant centrosomes to both defective mitosis (Mailand et al 2002) and multinucleation (Wonsey and Follettie 2005), both of which we show to occur following mutant p53 induction. The increased distance observed between centrosomes in mutant p53 expressing cells may be due to de-regulation of β-catenin as wild-type p53 inhibits β-catenin, with high β-catenin levels associated with mutant p53 expression and centrosome splitting (Hadjihannas et al 2010, Sadot et al 2001).

Our findings are consistent with observations of mutant p53 GOF in mouse models where the expression of the mouse R172H mutant (equivalent to human R175H) results in tumours exhibiting centrosome amplification and an associated aneuploidy (Caulin et al 2007, Hingorani et al 2005, Murphy et al 2000). However, these previous reports are confounded as they use a K-Ras^{G12D} mutation as an initiating oncogenic event (Caulin et al 2007, Hingorani et al 2005). Our data shows that mutant p53 alone is sufficient to drive the observed GOF phenotype. These mitotic defects would provide a likely origin for chromosomal instability, a common

feature of many human tumours, which promotes metastases and is correlated with poor patient prognosis (Kuukasjarvi et al 1997, Rajagopalan and Lengauer 2004).

This study has uncovered several novel genes and biological processes regulated by mutant p53 that regulate cellular movement and cell-to-cell signaling and interaction (Table 1). R175H has previously been shown to reprogram the cellular transcriptome through recruitment to novel target genes by various transcription factors, such as NF-Y (Di Agostino et al 2006), VDR (Stambolsky et al 2010) and NF-κβ (Schneider et al 2010). Indeed, our pathway analysis also showed that the NF-κβ signaling pathway was strongly up-regulated upon induced expression of p53-R175H (Figure S5B), further confirming a role for NF-κβ in the GOF of mutant p53 (Weisz et al 2007). Interestingly, several integrins (ITGA3 and ITGB3) were also up-regulated upon induction of p53-R175H consistent with a previously observed role for integrin recycling in the oncogenic GOF of mutant p53 (Muller et al 2009).

It has previously been shown that H1299 cells with inducible expression of p53-R175H exhibit a mesenchymal-like phenotype following TGFβ treatment (Adorno et al 2009). We observe this morphological change upon induction of both structural (R175H) and DNA contact (R248Q) p53 mutants with no additional treatment (Fig. 4A). Variations in cell density may account for this contradiction to previous data, as cells plated at higher densities did not exhibit this phenotype following mutant p53 induction (data not shown).

Mutant p53 GOF activity results in enhanced cellular migration, invasion and metastasis. We demonstrate that stable expression of ANKRD11 in the EI p53-R175H

cell line can suppress mutant p53-dependent invasion (Fig. 5). Furthermore, ANKRD11 is demonstrated to reduce the rate of migration of the MDA-MB-468 breast cancer cell line, expressing the endogenous p53-R273H mutant, in a mutant p53-dependent manner (Supp. Fig. S8). Silencing of mutant p53 expression has no effect on cell migration, which is consistent with previous reports showing that silencing of endogenous mutant p53 expression alone does not alter cellular migration in the MDA-MB-231 breast cancer cell line (Adorno et al 2009). However, expression of wild-type p53 has been demonstrated to inhibit cell migration (Gadea et al 2002, Roger et al 2006). Therefore, the observation that stable ANKRD11 expression can decrease the rate of cell migration in a mutant p53-dependent manner is likely due to a restoration of wild-type like activity to the endogenous p53 mutant, as previously described (Neilsen et al 2008).

For each of the assays described, the expression of ANKRD11 with induced mutant p53 restores the cellular phenotype to that seen in the uninduced state i.e. ANKRD11 suppresses the GOF of mutant p53. We have also established that ANKRD11 can restore wild-type p53 activity to p53 mutants. These data represent the first reported evidence of an endogenously expressed protein that has the capacity to suppress mutant p53 GOF as well as restore transcriptional activity to a p53 mutant (Neilsen et al 2008). This has broad implications for the development of new cancer therapies designed to target this pathway, as these may result not only in suppression of the invasive and metastatic properties of mutant p53 tumours, but also prevent tumour growth through a restoration of wild-type p53 activity.

We propose that ANKRD11 suppresses mutant p53 GOF by directly interacting with mutant p53 proteins resulting in a native wild-type p53 conformation (Fig. 6). This unique property of ANKRD11 is similar to that reported for small molecules and peptides PRIMA-1 (Bykov et al 2002) and CDB-3 (Friedler et al 2002, Issaeva et al 2003) which reportedly restore a native conformation to mutant p53. We also show that expression of the ANKRD11 ankyrin domain is sufficient to dissociate the p53-R175H•p63 and p53-R175H•p73 complexes (Fig. 7). The ability of mutant p53 to drive tumourigenesis is reported to be partially based on its ability to sequester the p63 and p73 proteins, thus disrupting their function to suppress metastasis (Di Como et al 1999, Gaiddon et al 2001). It is likely that ANKRD11 is suppressing mutant p53 GOF through an interaction with the C-terminus of p53 (Supp. Fig. S9) coupled with its ability to enhance the acetylation of the DNA binding domain (Neilsen et al 2008), thus leading to a stabilised, active conformation of p53 and subsequent dissociation of the mutant p53•p63/p73 complexes. Alternatively, the C-terminus of p53 has been shown to be required for mutant p53 invasive activity (Muller et al 2009), therefore we speculate that ANKRD11 may be out competing the recruitment of another unknown oncogenic protein required for mutant p53 GOF.

Studies defining mutant p53 interactions with p63 and p73 have included different subsets of mutants with the predominant focus on p53-R175H and p53-R273H (Gaiddon et al 2001, Strano et al 2000, Strano et al 2002). In this study we present a comprehensive comparison of the interaction of eight p53 hotspot mutants with p63 and p73, and show the structural class of mutants preferentially interact with both p63 and p73 with R273H the only DNA contact mutant shown to interact (Fig. 7), which is consistent with previous studies (Gaiddon et al 2001, Strano et al 2002).

A previously reported interaction between p63 and R248W (Gaiddon et al 2001) was not observed in this study. These data and others suggest a correlation between the structural integrity of the p53 protein and its ability to interact with p63/p73 (Gaiddon et al 2001). Interestingly, the endogenous p53-R273H mutant is reported to be immunoprecipitated from cell lines with the mutant specific antibody, PAb240 (Muller et al 2008), suggesting p53-R273H exhibits some structural perturbations. Furthermore, no interaction with p63 or p73 was observed for p53-R273C, suggesting that the amino acid at codon 273 plays an integral role in this interaction. In contrast to other structural mutants, G245S did not interact with p63 or p73 (Fig. 7). However, the p53-G245S protein is only local distorted in comparison to p53-R175H and p53-R282W that are globally distorted (Brosh and Rotter 2009, Wong et al 1999). These findings suggest that the extent of mutant p53 protein distortion may also dictate its ability to sequester p63 and p73.

The DNA contact mutants R248W and R248Q are shown to have a GOF in relation to multinucleation (Fig. 2A) and cellular morphology (Fig. 4A) respectively, however these mutants did not interact with p63 or p73. Therefore these mutants acquire their GOF independently of p63 or p73, presumably through interactions with other regulatory proteins. Possible candidates include the DNA repair complex protein MRE11. The specific interaction between MRE11 and the R248W mutant is reported to inactivate ATM, thereby inducing genetic instability (Liu et al 2010, Song et al 2007).

This study provides novel insight into the complex oncogenic processes that are driven by mutant p53. The discovery of ANKRD11 as an endogenously expressed

protein with the capacity to suppress various mutant p53 functions as well as restore wild-type activity to p53 mutants, opens a novel avenue to indirectly restore tumour suppressor activity to the guardian of the genome.

Materials and Methods

Cell Lines and Antibodies

H1299, MDA-MB-231, MCF-7 and SK-BR-3 cells were maintained in DMEM or RPMI with 10% FCS. Ecdysone-inducible derivatives of the H1299 cells were generated by stable transfection of pVgRXR and selection in zeocin (Invitrogen, CA) at 100 μg/ml, followed by stable transfection of pI-TK-Hygro-p53-wt/mut plasmid linearised with *Xba*I and subsequent selection of clones in Hygromycin B (Sigma Aldrich, St. Louis, MO) at 600 μg/ml. Stable cell lines expressing GFP-ANKRD11-Myc were generated through retroviral transduction using pLNCX2 vector as described previously (Neilsen et al 2008) and selected in G418 (Invitrogen) at 500 μg/ml. Antibodies used were: mouse α-Myc, mouse α-FLAG, mouse α-p53 DO-1 (Santa Cruz Biotechnology, Santa Cruz, CA), rat α-HA (Roche), rabbit α-β tubulin (Abcam), mouse α-β actin (Sigma Aldirch), mouse α-p21 (Thermo Scientific), mouse α-ZO-1 (Zymed), mouse α-Centrin, rabbit α-γ tubulin (Sigma), mouse α-MPM2 (Upstate), α-mouse IgG HRP linked (GE Healthcare), α-rabbit IgG HRP linked (GE Healthcare), α-rat IgG HRP linked (Dako, Carpinteria, CA), mouse light chain specific HRP linked (Millipore, Temecula, CA).

Plasmids

To generate epitope tagged fragments of ANKRD11, specific regions of ANKRD11 were PCR amplified using primers 1 to 8 (Table S1) from pLNCX2-ANKRD11-Myc (Neilsen et al 2008) and cloned in-frame into mammalian expression vectors pCMV-Tag2 or pCMV-Myc. Myc-p53-FL were generated as previously described (Neilsen et al 2008). Specific fragments of p53 were PCR amplified using primers 9 to 14 (Table S1) and cloned in frame into pCMV-Myc. Deletion constructs

of Myc-p53 were generated through overlap PCR using the primers 15 to 19 (Table S1).

Breast tumour analysis, expression microarray analysis and real-time RT-PCR

Breast tumour patient samples and real time PCR are as previously described (Kumar et al 2005, Pishas et al 2010). Expression profiling was performed using Affymetrix Human Gene 1.0 ST array as per manufacturer's protocol.

Co-Immunoprecipitation Assays

H1299 cells (5×10^5) were seeded into 60 mm dishes and transfected with the indicated constructs using Lipofectamine 2000 (Invitrogen). For the interaction domain mapping studies, cells were collected 24 hours post-transfection, resuspended in lysis buffer 1 (50 mM Tris-HCl pH 8, 150 mM NaCl, 1% Triton X-100) supplemented with 1× complete protease inhibitor cocktail (Roche), sonicated and centrifuged. Clarified lysates were incubated with FLAG-M2 agarose (Sigma) for 2 hours at 4ºC with rotation. Beads were washed twice with lysis buffer 1, twice with wash buffer (50 mM Tris-HCl pH 8, 150 mM NaCl, 1% NP-40, 0.5% sodium deoxycholate, 0.1% SDS) and twice with 20mM Tris-HCl pH 7.5. Protein complexes were eluted with FLAG peptide (200 ng/mL). For the p63/p73 interaction studies, cells were sequentially transfected with the indicated plasmids and harvested 48 hours post-transfection in 300µL lysis buffer 2 (20 mM Tris-HCl pH 8, 1 mM EDTA, 0.5% NP-40, 150 mM NaCl, 1 mM DTT, 10% glycerol), sonicated and centrifuged. Clarified lysates were incubated with 200 ng α-p53 (DO-1) for 1 hour at 4ºC with rotation, followed by addition of 10 µL Protein G sepharose beads (GE Healthcare) for 1 hour. Beads were washed four times with 400 µL lysis buffer 2 and protein

complexes were eluted with 1×SDS loading buffer at 95ºC for 5 min. Western blot analysis of inputs and co-immunoprecipitated protein complexes was performed as described previously (Kumar et al 2005).

Centrosome defects and multinucleation assays

To measure centrosome defects, unsynchronised cells were plated at 10% confluency and treated with 2.5 μg/mL PonA for the indicated times. Multinucleation, number of centrosomes and centrosome size was measure in interphase cells. Distance between centrosomes was measured in S and G2 cells. 50 cells were counted per condition. For mitotic assays, cells were plated at 10% confluency, synchronised by double thymidine block and harvested at 11 hours post-release. 2.5 μg/mL PonA was added 24 hours before harvesting. 100 cells were counted per condition.

Colony development assays

EI p53-mut cell lines were treated with or without 2.5 μg/mL PonA for 72 hrs. Cells were subsequently collected and plated in duplicate in a 6-well format at 1000 cells/well in DMEM ± PonA. Cells were grown for 10 days, fixed for 5 minutes with methanol and stained with Giemsa Stain (Sigma Aldrich) as per manufacturer's protocol.

Immunofluorescence

For ZO-1 staining, 2000 cells were plated on glass coverslips in a 6-well and allowed to form small colonies of 4-6 cells (~2 days). PonA was added to wells at a final concentration of 2.5 μg/mL for 0, 16 or 40hrs. IF protocols were based on those previously described (Neilsen et al 2008).

For mitotic staining, cells were synchronised by addition of 2.5 mM thymidine for 16 hours then washed three times in PBS. Cells were incubated for a further 10 hours before the thymidine block was repeated. Cells were fixed with ice-cold methanol at 11 hours post-release from the second thymidine block. PonA was added at 24 hours prior to harvesting. Where metaphase cells were required 10 μM MG132 was added at two hours prior to harvesting. Cells were blocked in 3% BSA in PBS for 20 minutes followed by incubation with the indicated antibodies in 03% BSA/PBS solution (30 minutes, RT), and incubation with the indicated Alexa-Fluor-conjugated secondary antibodies (30 minutes, RT). Coverslips were mounted in mowiol containing 2.5% DABCO. Cells were visualised using a DeltaVision personal DV deconvolution microscope. Images underwent restoration deconvolution and were analysed using softWoRx version 3.6.1. Fluorescent images represent projections of z-stacks. Images were cropped and resized using Adobe Photoshop (San Jose, CA, USA).

Invasion Assays

Real-time invasion assays were performed using the xCelligence Real-Time Cell Analyzer (RTCA) DP (Roche), as per the manufacturer's protocol. Ecdysone-inducible H1299 derivatives, EI-H1299-p53-R175H or EI-H1299-p53-R175H-ANKRD11 were grown in the presence or absence of PonA at 2.5μg/ml for 24 hours. Following induction, sub-confluent cell cultures were collected in serum free media and plated at 2×10^4 cells per well in the top chamber of a CIM-Plate 16 pre-coated with 5% Matrigel (BD Biosciences, San Jose, CA). DMEM containing 10% FCS was used as a chemo-attractant. Real-time migration assays were performed using

Incucyte (Essen). Phase images were taken every 30 minutes and wound closure and cell confluence calculated using specific Incucyte software.

Live cell imaging

Live cell imaging was conducted using a DeltaVision Core microscope using softWoRx version 3.6.1. Cells were plated at 10% confluency, synchronised by double thymidine block and 2.5 μg/mL PonA added 24 hours before imaging. Bright field images were taken every five minutes and the movies analysed using ImageJ version 1.43u.

Statistical Testing

Significance testing for breast tumour data was performed using a two-tailed Student's t-test. Two-Way ANOVA and Bonferroni posttests were performed using GraphPad Prism (v5, CA, USA).

Conflict of interest

The authors declare no conflict of interest.

Acknowledgements

We would like to thank Vivek Mittal for ecdysone-inducible constructs, Karen Vousden and Patricia Muller for p63 and p73 constructs, Maria Lung, Sumitra Deb and Chikashi Ishioka for mutant p53 constructs, Jeffrey Salisbury for the anti-centrin antibody, Anne-Marie Cleton-Jansen for providing patient material and Darryl Russell and Kira Height for technical assistance. We wish to acknowledge the Cancer Council of South Australia and San Remo for their financial support. K.K.K is a National

Health and Medical Research Council (NHMRC) Senior Principal Research Fellow and this work is supported by NHMRC Program grant to K.K.K. F.A is supported by the Cancer Council NSW, the Cure Cancer Foundation Australia and the Cancer Council SA.

Supplementary material is available at Oncogene's website.

References

Adorno M, Cordenonsi M, Montagner M, Dupont S, Wong C, Hann B *et al* (2009). A Mutant-p53/Smad complex opposes p63 to empower TGFbeta-induced metastasis. *Cell* **137:** 87-98.

Brosh R, Rotter V (2009). When mutants gain new powers: news from the mutant p53 field. *Nat Rev Cancer* **9:** 701-713.

Bullock AN, Fersht AR (2001). Rescuing the function of mutant p53. *Nat Rev Cancer* **1:** 68-76.

Bykov VJ, Issaeva N, Shilov A, Hultcrantz M, Pugacheva E, Chumakov P *et al* (2002). Restoration of the tumor suppressor function to mutant p53 by a low-molecular-weight compound. *Nat Med* **8:** 282-288.

Caulin C, Nguyen T, Lang GA, Goepfert TM, Brinkley BR, Cai WW *et al* (2007). An inducible mouse model for skin cancer reveals distinct roles for gain- and loss-of-function p53 mutations. *J Clin Invest* **117:** 1893-1901.

Cho Y, Gorina S, Jeffrey PD, Pavletich NP (1994). Crystal structure of a p53 tumor suppressor-DNA complex: understanding tumorigenic mutations. *Science* **265:** 346-355.

Di Agostino S, Strano S, Emiliozzi V, Zerbini V, Mottolese M, Sacchi A *et al* (2006). Gain of function of mutant p53: the mutant p53/NF-Y protein complex reveals an aberrant transcriptional mechanism of cell cycle regulation. *Cancer Cell* **10:** 191-202.

Di Agostino S, Cortese G, Monti O, Dell'Orso S, Sacchi A, Eisenstein M *et al* (2008). The disruption of the protein complex mutantp53/p73 increases selectively the response of tumor cells to anticancer drugs. *Cell Cycle* **7:** 3440-3447.

Di Como CJ, Gaiddon C, Prives C (1999). p73 function is inhibited by tumor-derived p53 mutants in mammalian cells. *Mol Cell Biol* **19:** 1438-1449.

Dong P, Xu Z, Jia N, Li D, Feng Y (2009). Elevated expression of p53 gain-of-function mutation R175H in endometrial cancer cells can increase the invasive phenotypes by activation of the EGFR/PI3K/AKT pathway. *Mol Cancer* **8:** 103.

Friedler A, Hansson LO, Veprintsev DB, Freund SM, Rippin TM, Nikolova PV *et al* (2002). A peptide that binds and stabilizes p53 core domain: chaperone strategy for rescue of oncogenic mutants. *Proc Natl Acad Sci U S A* **99:** 937-942.

Gadea G, Lapasset L, Gauthier-Rouviere C, Roux P (2002). Regulation of Cdc42-mediated morphological effects: a novel function for p53. *EMBO J* **21:** 2373-2382.

Gaiddon C, Lokshin M, Ahn J, Zhang T, Prives C (2001). A subset of tumor-derived mutant forms of p53 down-regulate p63 and p73 through a direct interaction with the p53 core domain. *Mol Cell Biol* **21:** 1874-1887.

Hadjihannas MV, Bruckner M, Behrens J (2010). Conductin/axin2 and Wnt signalling regulates centrosome cohesion. *EMBO Rep* **11:** 317-324.

Hansen LL, Yilmaz M, Overgaard J, Andersen J, Kruse TA (1998). Allelic loss of 16q23.2-24.2 is an independent marker of good prognosis in primary breast cancer. *Cancer Res* **58:** 2166-2169.

Hingorani SR, Wang L, Multani AS, Combs C, Deramaudt TB, Hruban RH *et al* (2005). Trp53R172H and KrasG12D cooperate to promote chromosomal instability and widely metastatic pancreatic ductal adenocarcinoma in mice. *Cancer Cell* **7:** 469-483.

Hollstein M, Sidransky D, Vogelstein B, Harris CC (1991). p53 mutations in human cancers. *Science* **253:** 49-53.

Issaeva N, Friedler A, Bozko P, Wiman KG, Fersht AR, Selivanova G (2003). Rescue of mutants of the tumor suppressor p53 in cancer cells by a designed peptide. *Proc Natl Acad Sci U S A* **100:** 13303-13307.

Kato S, Han SY, Liu W, Otsuka K, Shibata H, Kanamaru R *et al* (2003). Understanding the function-structure and function-mutation relationships of p53 tumor suppressor protein by high-resolution missense mutation analysis. *Proc Natl Acad Sci U S A* **100:** 8424-8429.

Kravchenko JE, Ilyinskaya GV, Komarov PG, Agapova LS, Kochetkov DV, Strom E *et al* (2008). Small-molecule RETRA suppresses mutant p53-bearing cancer cells through a p73-dependent salvage pathway. *Proc Natl Acad Sci U S A* **105:** 6302-6307.

Kumar R, Neilsen PM, Crawford J, McKirdy R, Lee J, Powell JA *et al* (2005). FBXO31 is the chromosome 16q24.3 senescence gene, a candidate breast tumor suppressor, and a component of an SCF complex. *Cancer Res* **65:** 11304-11313.

Kuukasjarvi T, Karhu R, Tanner M, Kahkonen M, Schaffer A, Nupponen N *et al* (1997). Genetic heterogeneity and clonal evolution underlying development of asynchronous metastasis in human breast cancer. *Cancer Res* **57:** 1597-1604.

Lane DP (1992). Cancer. p53, guardian of the genome. *Nature* **358:** 15-16.

Liu DP, Song H, Xu Y (2010). A common gain of function of p53 cancer mutants in inducing genetic instability. *Oncogene* **29:** 949-956.

Liu G, Chen X (2006). Regulation of the p53 transcriptional activity. *J Cell Biochem* **97:** 448-458.

Mailand N, Lukas C, Kaiser BK, Jackson PK, Bartek J, Lukas J (2002). Deregulated human Cdc14A phosphatase disrupts centrosome separation and chromosome segregation. *Nat Cell Biol* **4:** 317-322.

Miller LD, Smeds J, George J, Vega VB, Vergara L, Ploner A *et al* (2005). An expression signature for p53 status in human breast cancer predicts mutation status,

transcriptional effects, and patient survival. *Proc Natl Acad Sci U S A* **102:** 13550-13555.

Milner J, Cook A, Sheldon M (1987). A new anti-p53 monoclonal antibody, previously reported to be directed against the large T antigen of simian virus 40. *Oncogene* **1:** 453-455.

Muller P, Hrstka R, Coomber D, Lane DP, Vojtesek B (2008). Chaperone-dependent stabilization and degradation of p53 mutants. *Oncogene* **27:** 3371-3383.

Muller PA, Caswell PT, Doyle B, Iwanicki MP, Tan EH, Karim S *et al* (2009). Mutant p53 drives invasion by promoting integrin recycling. *Cell* **139:** 1327-1341.

Murphy KL, Dennis AP, Rosen JM (2000). A gain of function p53 mutant promotes both genomic instability and cell survival in a novel p53-null mammary epithelial cell model. *FASEB J* **14:** 2291-2302.

Neilsen PM, Cheney KM, Li CW, Chen JD, Cawrse JE, Schulz RB *et al* (2008). Identification of ANKRD11 as a p53 coactivator. *J Cell Sci* **121:** 3541-3552.

Olivier M, Hollstein M, Hainaut P (2010). TP53 mutations in human cancers: origins, consequences, and clinical use. *Cold Spring Harb Perspect Biol* **2:** a001008.

Oren M, Rotter V (2010). Mutant p53 gain-of-function in cancer. *Cold Spring Harb Perspect Biol* **2:** a001107.

Pishas KI, Al-Ejeh F, Zinonos I, Kumar R, Evdokiou A, Brown MP *et al* (2010). Nutlin-3a is a potential therapeutic for Ewing Sarcoma. *Clin Cancer Res*.

Rajagopalan H, Lengauer C (2004). Aneuploidy and cancer. *Nature* **432:** 338-341.

Roger L, Gadea G, Roux P (2006). Control of cell migration: a tumour suppressor function for p53? *Biol Cell* **98:** 141-152.

Sadot E, Geiger B, Oren M, Ben-Ze'ev A (2001). Down-regulation of beta-catenin by activated p53. *Mol Cell Biol* **21:** 6768-6781.

Schneider G, Henrich A, Greiner G, Wolf V, Lovas A, Wieczorek M *et al* (2010). Cross talk between stimulated NF-kappaB and the tumor suppressor p53. *Oncogene* **29:** 2795-2806.

Scian MJ, Stagliano KE, Deb D, Ellis MA, Carchman EH, Das A *et al* (2004). Tumor-derived p53 mutants induce oncogenesis by transactivating growth-promoting genes. *Oncogene* **23:** 4430-4443.

Song H, Hollstein M, Xu Y (2007). p53 gain-of-function cancer mutants induce genetic instability by inactivating ATM. *Nat Cell Biol* **9:** 573-580.

Stambolsky P, Tabach Y, Fontemaggi G, Weisz L, Maor-Aloni R, Siegfried Z *et al* (2010). Modulation of the vitamin D3 response by cancer-associated mutant p53. *Cancer Cell* **17:** 273-285.

Strano S, Munarriz E, Rossi M, Cristofanelli B, Shaul Y, Castagnoli L *et al* (2000). Physical and functional interaction between p53 mutants and different isoforms of p73. *J Biol Chem* **275:** 29503-29512.

Strano S, Fontemaggi G, Costanzo A, Rizzo MG, Monti O, Baccarini A *et al* (2002). Physical interaction with human tumor-derived p53 mutants inhibits p63 activities. *J Biol Chem* **277:** 18817-18826.

Vogelstein B, Lane D, Levine AJ (2000). Surfing the p53 network. *Nature* **408:** 307-310.

Weisz L, Damalas A, Liontos M, Karakaidos P, Fontemaggi G, Maor-Aloni R *et al* (2007). Mutant p53 enhances nuclear factor kappaB activation by tumor necrosis factor alpha in cancer cells. *Cancer Res* **67:** 2396-2401.

Wong KB, DeDecker BS, Freund SM, Proctor MR, Bycroft M, Fersht AR (1999). Hot-spot mutants of p53 core domain evince characteristic local structural changes. *Proc Natl Acad Sci U S A* **96:** 8438-8442.

Wonsey DR, Follettie MT (2005). Loss of the forkhead transcription factor FoxM1 causes centrosome amplification and mitotic catastrophe. *Cancer Res* **65:** 5181-5189.

Figure Legends

Figure 1. ANKRD11 is down-regulated in breast tumours and is predictive of poor clinical outcome

A: ANKRD11 expression levels were determined by quantitative real-time PCR in 38 breast tumours and 2 normal breast tissues.

B: Kaplan-Meier curves derived from publically available survival data associated with a cohort of 246 breast cancer patients with known p53 status (GSE3494; (Miller et al 2005)). Expression of ANKRD11 was sourced from expression microarray analyses. Tumours were ranked by ANKRD11 expression, with the lowest 15% of these tumours defined as 'Low ANKRD11'.

C: Two-by-two test (Fisher's exact test) showing a correlation between lymph node status of a cohort of 53 patients with mutant p53 expressing breast tumours (GSE3494; (Miller et al 2005)) and ANKRD11 expression (as defined in B).

Figure 2. Mutant p53 expression promotes multinucleation and centrosome abnormalities that are suppressed by ANKRD11

EI p53-WT, EI p53-R248W, EI p53-R175H, EI p53-R249S and EI p53-R175H-ANKRD11 were plated at 10% confluency and treated with 2.5μg/mL PonA for 0, 24, 48, 72 or 96 hours. Multinucleation and centrosome characteristics were subsequently analysed. γ-tubulin was used as a centrosome marker for centrosome measurements. Error bars represent the SEM of three independent experiments; * $p < 0.05$, ** $p < 0.01$ and *** $p < 0.001$.

A: The percentage of multinucleated cells was determined using DAPI and α-tubulin staining. For each experiment 100 cells were counted per condition.

B: The average number of centrosomes per cell was determined in wt and p53 mutants at 24 hour intervals over 96 hours. For each experiment 40 cells were counted per condition.

C: The average centrosome size was determined in wt and p53 mutants at 24 hour intervals over 96 hours. For each experiment 40 cells were counted per condition. Where two or more centrosomes were present the largest centrosome was measured.

D: The average distance between centrosomes was determined in wt and p53 mutants at 24 hour intervals over 96 hrs. For each experiment 40 cells were counted per condition. Where three or more centrosomes were present the largest distance between two neighbouring centrosomes was measured.

E: The level of wild-type or p53-R175H protein expressed following 24 hour induction in the presence or absence of ANKRD11 re-expression was determined by western blot analysis, with β-actin protein levels used as a loading control.

Figure 3. Induction of mutant p53 results in mitotic defects that are alleviated by ANKRD11 expression

EI p53-R248W, EI p53-R175H, EI p53-R249S and EI p53-R175H-ANKRD11 cells were plated at 10% confluency and synchronised by double thymidine block and harvested at 11 hours post-release. PonA was added at 24 hours before harvesting. For each experiment 100 cells were counted per condition. Error bars represent the SEM from three independent experiments; * $p < 0.05$, ** $p < 0.01$ and *** $p < 0.001$.

A: The average percentage of metaphase cells with abnormal spindles was determined using α-tubulin as a marker of the mitotic spindle. Cells were synchronised in metaphase by the addition of 10 μM MG132 at two hours prior to harvesting.

B: Representative images of the spindle morphology uninduced and induced cells. Cells were stained for α-tubulin (red), γ-tubulin (green) and DAPI (blue). Scale bar represents 20 μm.

C: The average percentage of anaphase/telophase cells with lagging chromosomes was determined using DAPI as a marker of the DNA.

D: The average percentage of daughter (newly divided) cells with anaphase bridges was determined using DAPI as a marker of the DNA.

E: The average time taken for cells to undergo mitosis. Synchronised cells were followed by time lapse microscopy and imaged every five minutes. Time in mitosis was defined as the time from nuclear envelope breakdown until the point at which two daughter cells could be seen. For each experiment 50 cells were counted per condition.

Figure 4. Induction of mutant p53 in H1299 cells results in an altered cellular phenotype, which is suppressed by ANKRD11

A: EI p53-R175H and EI p53-R248Q cells were untreated (left) or treated (middle) with 2.5 μg/mL PonA and plated at single cell density. Colonies were fixed and stained 10 days post-plating. Pictures show representative colonies. Each cell line with re-expressed ANKRD11 was treated in a similar manner (right).

B: The EI p53-R175H cell line were seeded at single cell density and allowed to develop into colonies for 72 hours prior to the addition of PonA (2.5 μg/mL) as indicated. Colonies were stained for the presence of cell-cell junctions, as indicated by ZO-1 staining (red).

Figure 5. ANKRD11 suppresses p53-R175H mediated invasion

A: EI p53-R175H or EI p53-R175H-ANKRD11 cells were treated as indicated with 2.5 μg/mL PonA for 24 hrs prior to plating in the upper chamber of a CIM-16 plate coated with 5% matrigel. Real-time invasion of cells was measured on an Xcelligence RTCA DP analyser.

B: The rate of invasion during the linear phase (between 15 and 24 hours) as determined by the gradient (n=4; * $p<0.05$).

Figure 6. ANKRD11 restores a native conformation to a p53 mutant

A: H1299 cells were sequentially transfected with 4 μg FLAG-ANKRD11$^{144\text{-}288aa}$ and 0.5 μg wild-type or mutant p53 expression constructs, followed by immunoprecipitation with an α-FLAG antibody. Inputs and immunoprecipitated complexes were subjected to western blot analysis with α-p53 and α-FLAG antibodies. All p53 mutants investigated are shown to co-precipitate with ANKRD11$^{144\text{-}288aa}$ above the level of non-specific, background levels seen in empty vector control lanes.

B: EI p53-R175H and EI p53-R175H-ANKRD11 cells were treated with 2.5 μg/mL PonA for 24 hours, immunoprecipitated with indicated antibody and detected by western blot analysis using α-p53 (DO-1) and α-mouse light chain-specific secondary antibody.

Figure 7. The ankyrin domain of ANKRD11 dissociates the p53-R175H•p63/p73 complexes

A: H1299 cells were co-transfected with 2 μg wild-type or mutant p53 expression constructs and 4 μg HA-p63. Cellular extracts were subjected to immunoprecipitation

with α-p53 (DO-1) antibody. Inputs and immunoprecipitates were subjected to western blot analysis using α-p53 and α-HA antibodies.

B: Cells were treated as described above (A) but p53 was co-transfected with HA-p73.

C: H1299 cells were sequentially transfected with 2 μg p53-R175H, 4 μg HA-p63 and 2 μg various Myc-ANKRD11 fragment expression constructs as indicated followed by immunoprecipitation with α-p53 (DO-1) antibody. Inputs and immunoprecipitates were subjected to western blot analysis with α-p53, α-Myc and α-HA antibodies. The amount of p63 co-precipitated with p53-R175H was determined by densitometry.

D: Cells were treated as above (C) but with HA-p73 and Myc-ANKRD11$^{144\text{-}288aa}$ expression constructs.

E: Schematic diagram illustrating the region of ANKRD11 capable of dissociating the mutant p53-p63 complex.

Figure 1

A

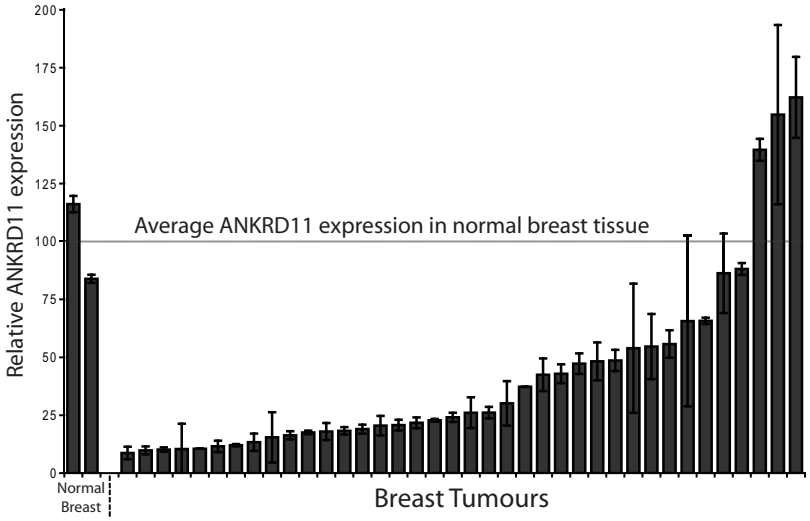

B

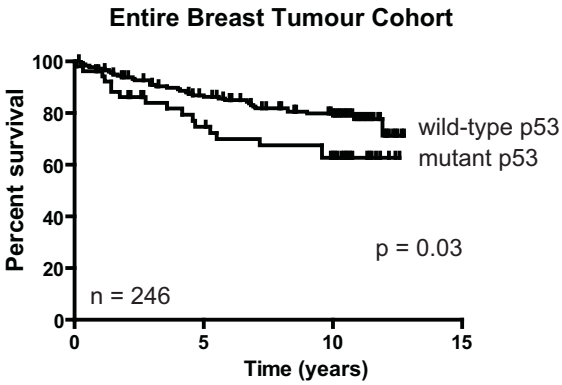

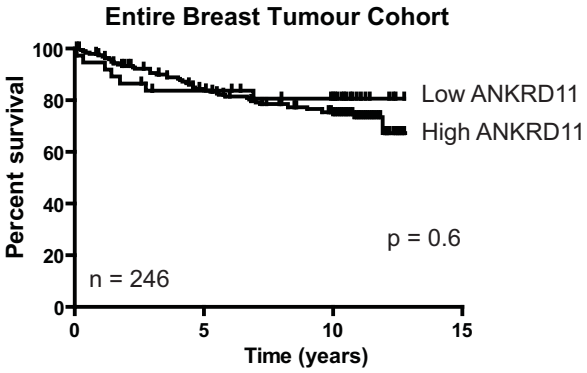

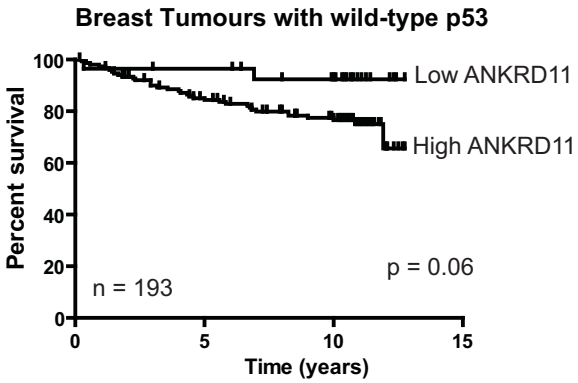

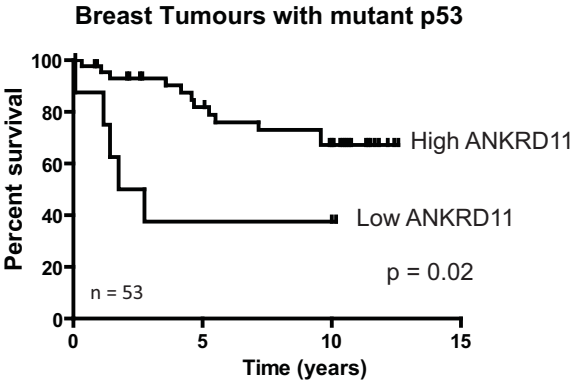

C

Breast tumours with mutant p53

	Lymph node negative	Lymph node positive
Low ANKRD11	1	7
High ANKRD11	32	13

Fisher's exact test

p = 0.003

n = 53

Figure 2

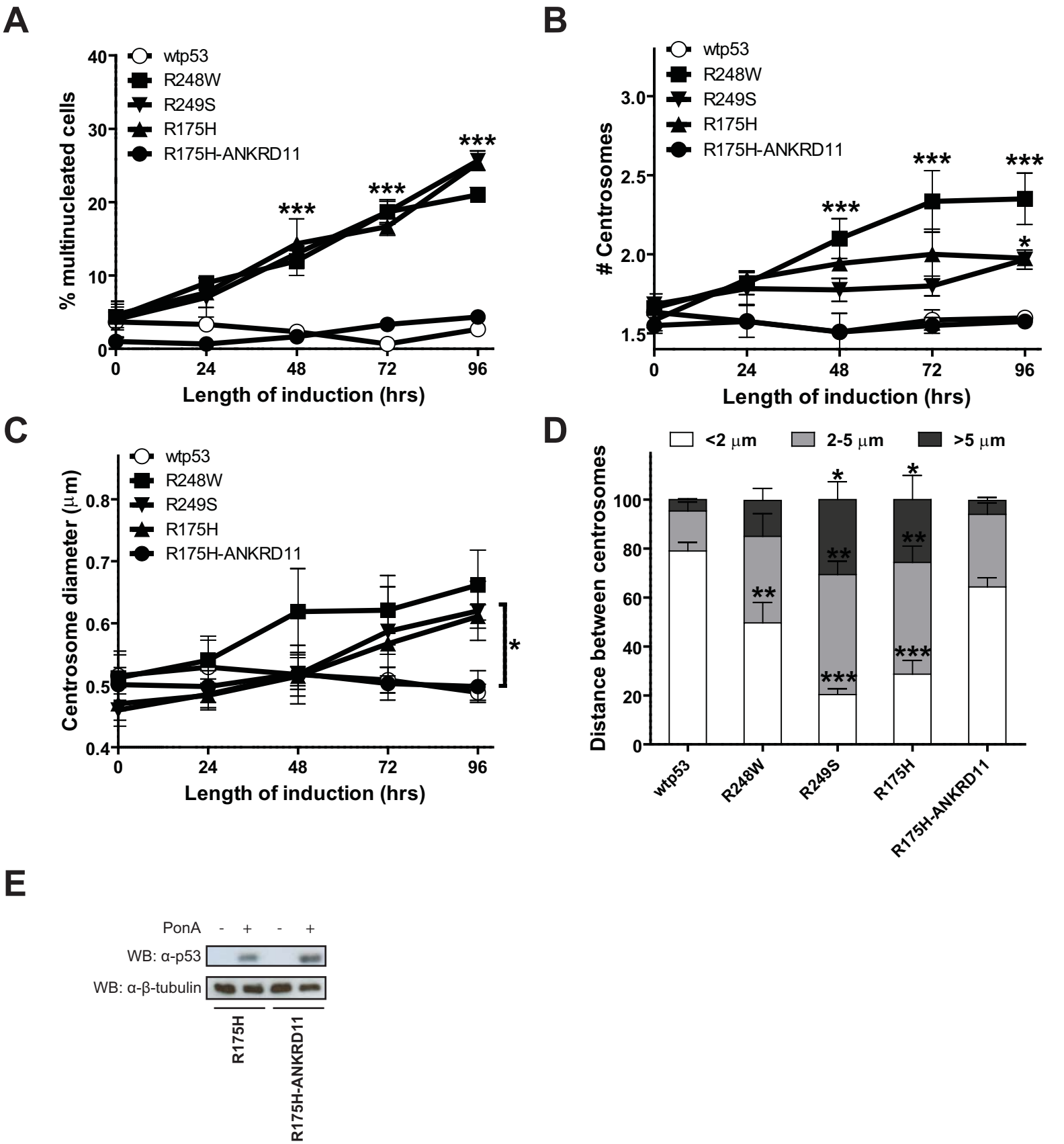
A
wtp53
R248W
R249S
R175H
R175H-ANKRD11
% multinucleated cells
Length of induction (hrs)
B
Centrosomes
Length of induction (hrs)
C
Centrosome diameter (μm)
Length of induction (hrs)
D
<2 μm
2-5 μm
>5 μm
Distance between centrosomes
wtp53
R248W
R249S
R175H
R175H-ANKRD11
E
PonA - + - +
WB: α-p53
WB: α-β-tubulin
R175H
R175H-ANKRD11

Figure 3

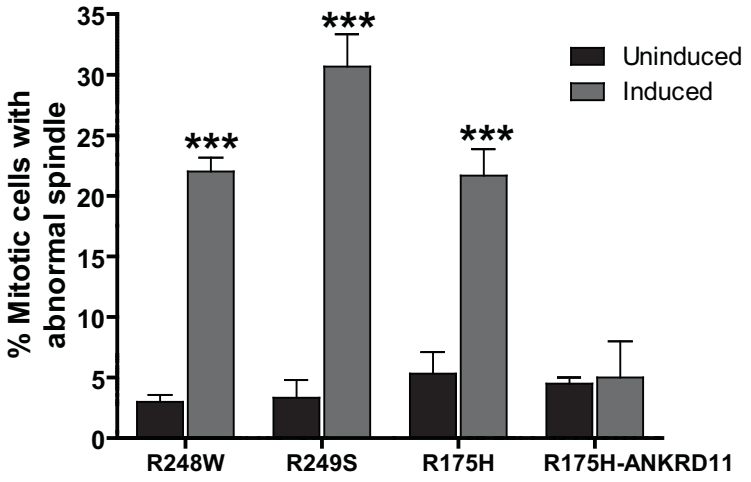
A
% Mitotic cells with abnormal spindle
35
30
25
20
15
10
5
0
***
***
***
Uninduced
Induced
R248W
R249S
R175H
R175H-ANKRD11

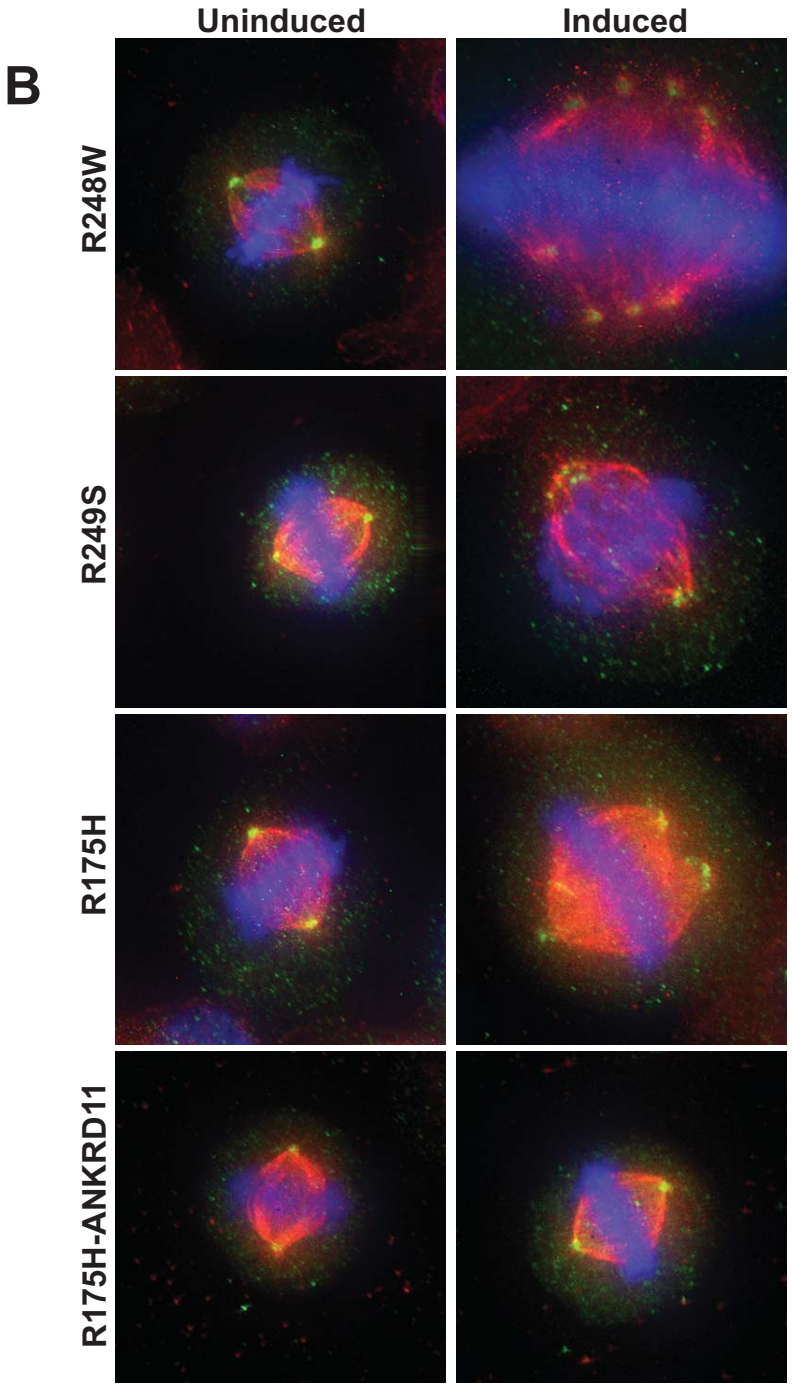
B
Uninduced
Induced
R248W
R249S
R175H
R175H-ANKRD11

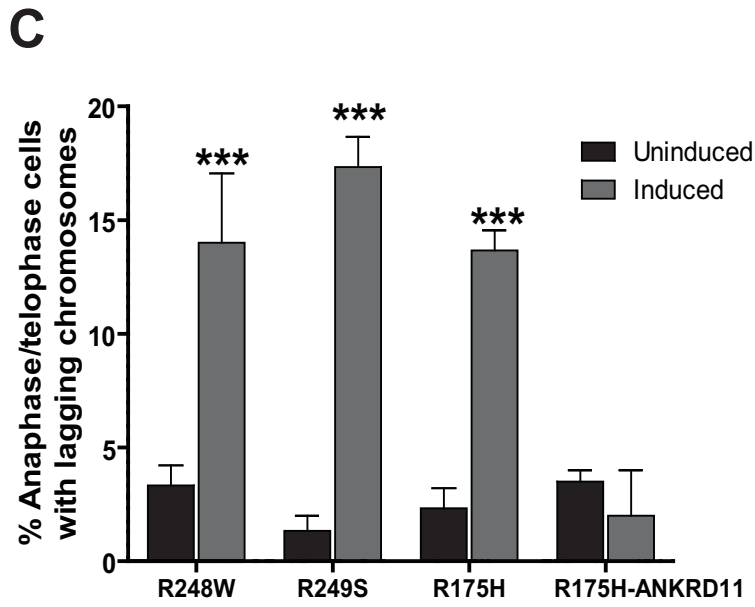
C
% Anaphase/telophase cells with lagging chromosomes
20
15
10
5
0
***
***
***
Uninduced
Induced
R248W
R249S
R175H
R175H-ANKRD11

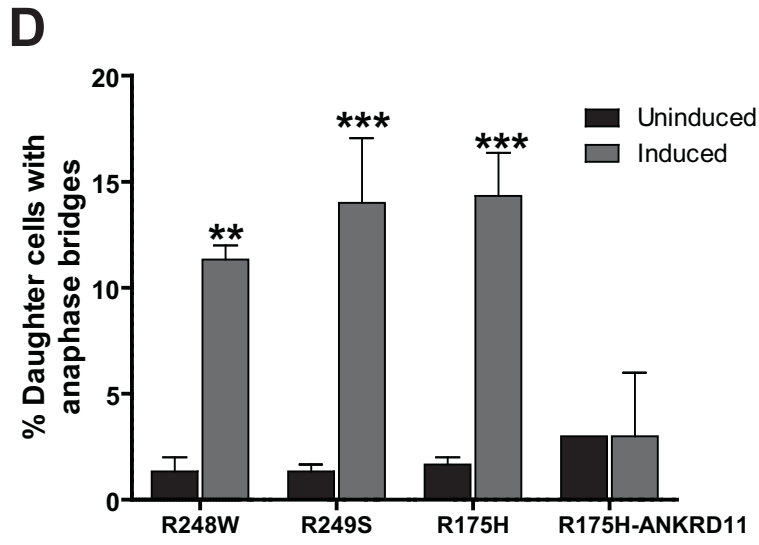
D
% Daughter cells with anaphase bridges
20
15
10
5
0
**
***
***
Uninduced
Induced
R248W
R249S
R175H
R175H-ANKRD11

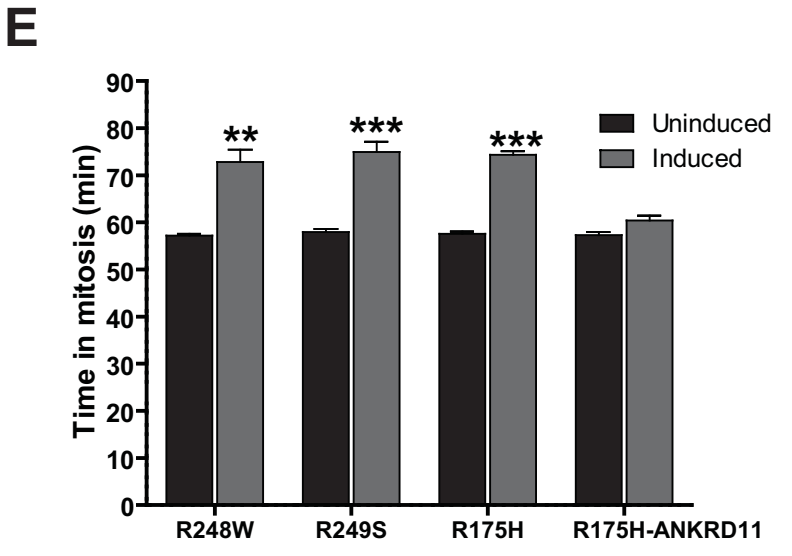
E
Time in mitosis (min)
90
80
70
60
50
40
30
20
10
0
**
***
***
Uninduced
Induced
R248W
R249S
R175H
R175H-ANKRD11

FIGURE 4

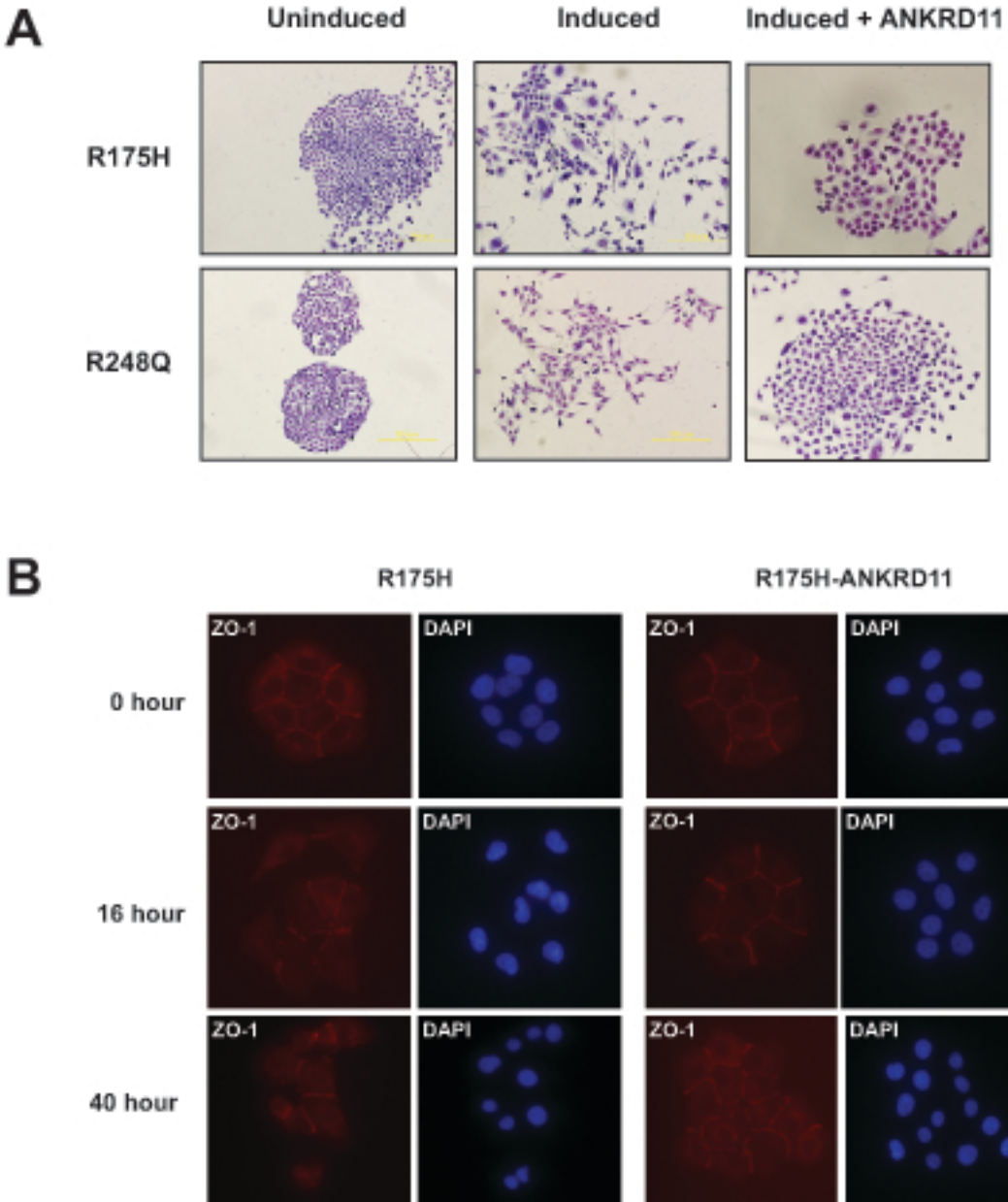
A
Uninduced
Induced
Induced + ANKRD11
R175H
R248Q
B
R175H
R175H-ANKRD11
ZO-1
DAPI
0 hour
16 hour
40 hour

Figure 5

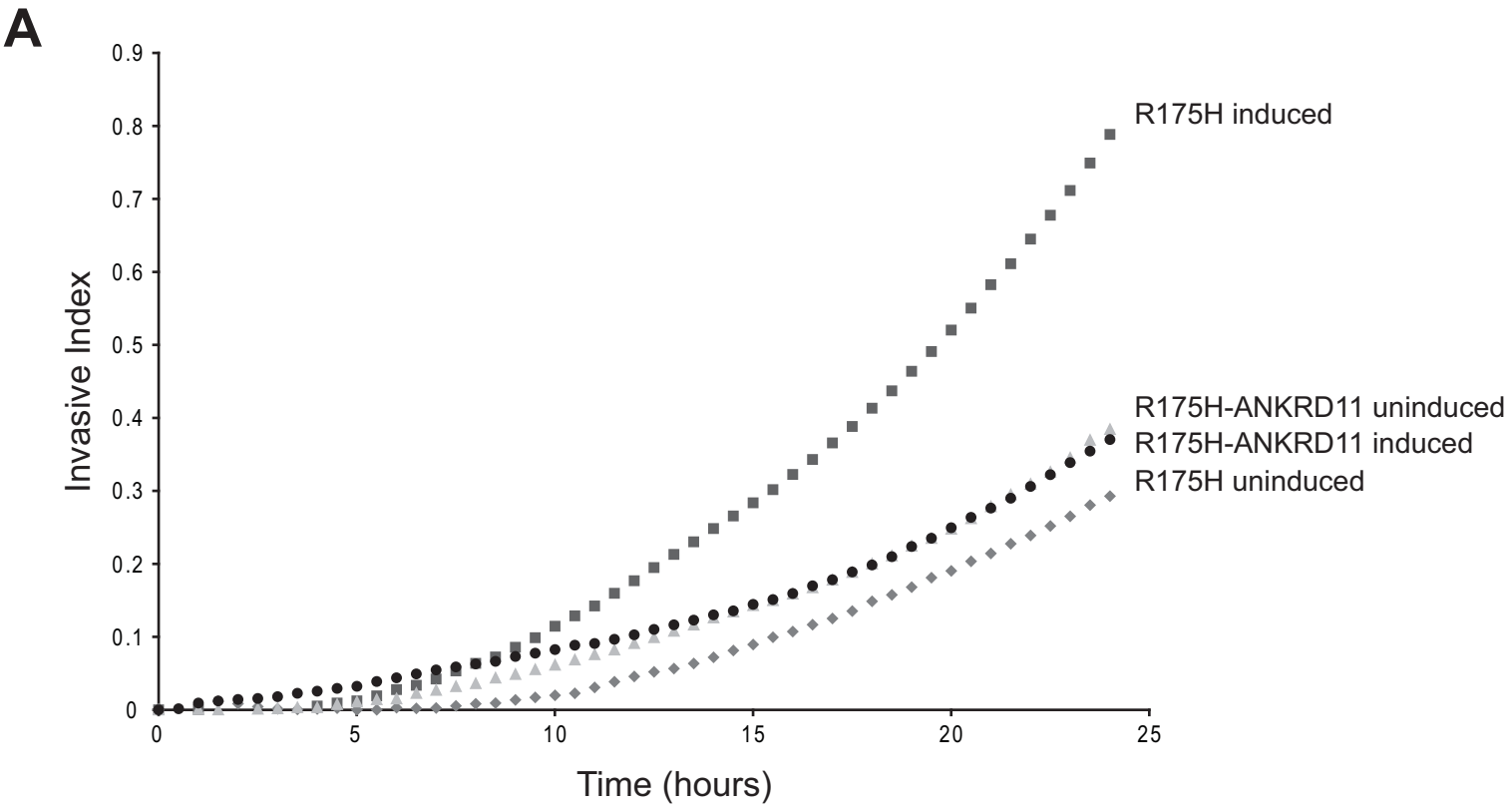
A
Invasive Index
Time (hours)
R175H induced
R175H-ANKRD11 uninduced
R175H-ANKRD11 induced
R175H uninduced
0
0.1
0.2
0.3
0.4
0.5
0.6
0.7
0.8
0.9
0
5
10
15
20
25

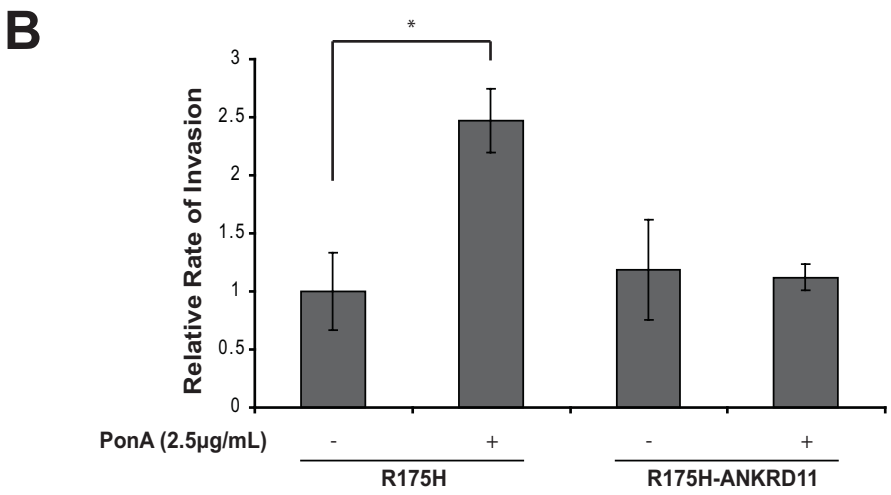
B
Relative Rate of Invasion
*
0
0.5
1
1.5
2
2.5
3
PonA (2.5µg/mL)
-
+
-
+
R175H
R175H-ANKRD11

Figure 6

A

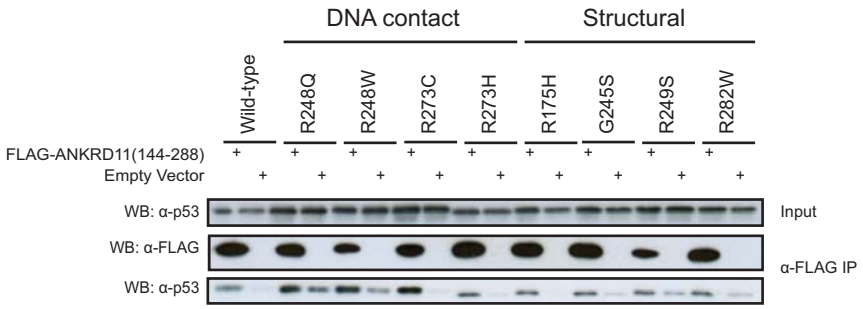
DNA contact
Structural
Wild-type
R248Q
R248W
R273C
R273H
R175H
G245S
R249S
R282W
FLAG-ANKRD11(144-288)
Empty Vector
WB: α-p53
WB: α-FLAG
WB: α-p53
Input
α-FLAG IP

B

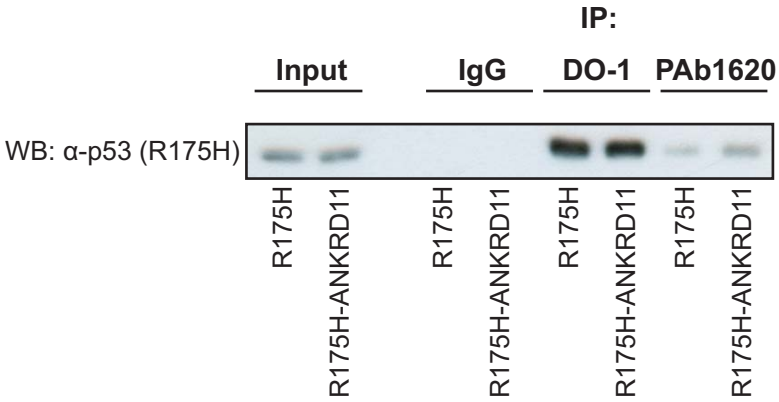
IP:
Input
IgG
DO-1
PAb1620
WB: α-p53 (R175H)
R175H
R175H-ANKRD11
R175H
R175H-ANKRD11
R175H
R175H-ANKRD11
R175H
R175H-ANKRD11

Figure 7

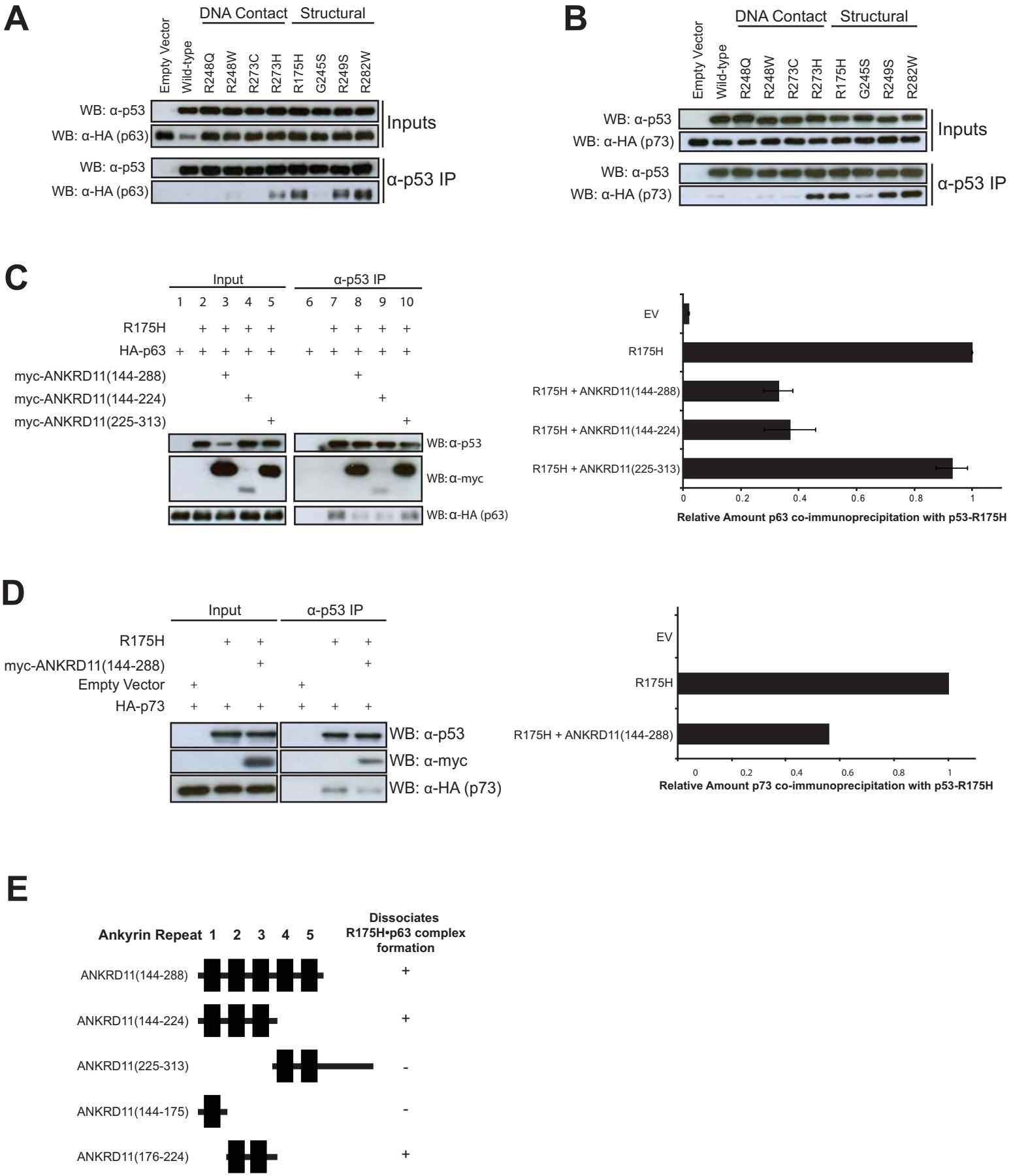
A
DNA Contact
Structural
Empty Vector
Wild-type
R248Q
R248W
R273C
R273H
R175H
G245S
R249S
R282W
WB: α-p53
WB: α-HA (p63)
Inputs
WB: α-p53
WB: α-HA (p63)
α-p53 IP
B
DNA Contact
Structural
Empty Vector
Wild-type
R248Q
R248W
R273C
R273H
R175H
G245S
R249S
R282W
WB: α-p53
WB: α-HA (p73)
Inputs
WB: α-p53
WB: α-HA (p73)
α-p53 IP
C
Input
α-p53 IP
1 2 3 4 5 6 7 8 9 10
R175H
HA-p63
myc-ANKRD11(144-288)
myc-ANKRD11(144-224)
myc-ANKRD11(225-313)
WB: α-p53
WB: α-myc
WB: α-HA (p63)
EV
R175H
R175H + ANKRD11(144-288)
R175H + ANKRD11(144-224)
R175H + ANKRD11(225-313)
0 0.2 0.4 0.6 0.8 1
Relative Amount p63 co-immunoprecipitation with p53-R175H
D
Input
α-p53 IP
R175H
myc-ANKRD11(144-288)
Empty Vector
HA-p73
WB: α-p53
WB: α-myc
WB: α-HA (p73)
EV
R175H
R175H + ANKRD11(144-288)
0 0.2 0.4 0.6 0.8 1
Relative Amount p73 co-immunoprecipitation with p53-R175H
E
Ankyrin Repeat 1 2 3 4 5
Dissociates R175H•p63 complex formation
ANKRD11(144-288) +
ANKRD11(144-224) +
ANKRD11(225-313) -
ANKRD11(144-175) -
ANKRD11(176-224) +

Table I. Genes regulated by induction of p53-R175H

Category	Function	p-value	Gene Names		Molecules
			Down-regulated	Up-regulated	
Cellular Movement	migration	1.69E-05	CD22, DLX2,	ANGPTL4, ANPEP, DKK1, ID2, ITGA3, ITGB3, KRT6A, LAMC2, MAP2K3, NR2F2, OPHN1, PDE2A, PPARG, RAC2, RALB, SEMA3C, SERPINA1, SFRP1, STC1, TGFBI, TNFSF4, TP53	24
Cancer	tumorigenesis	3.45E-05	CD22, CD274, SOCS2, STC1, TUBB2C, WEE1	ABCC3, AHCYL1, AKAP12, AKAP13, ANGPTL4, ANPEP, BCL2L1, CDA, CDH3, CPA4, DDIT4, DECR1, DKK1, EDNRA, EHHADH, FSTL3, ID2, ITGA3, ITGB3, KRT6A, LAMC2, RALB, SCD, SEMA3C, SERPINA1, SFRP1, SLC46A3, LRIG1, MAP2K3, MT1X, OGG1, PDE2A, PLK2, PPARG, PRDM1, PRSS12, PSD3, PTX3, TFPI2, TP53	46
Cell Death	cell death	7.01E-05	ATG12, CD22, CD274, DLX2, WEE1	AKAP12, ANGPTL4, ANPEP, ATXN1, BCL2L1, CTH, DDIT4, DECR1, DKK1, FSTL3, GLIPR1, ID2, ITGB3, LRIG1, MAP2K3, MT1X, OGG1, P2RX4, PLK2, PPARG, PRDM1, RAC2, RALB, SCD, SERPINA1, SFRP1, SRR, TFPI2, TGFBI, TP53, UQCRFS1, VIPR2	37
Cell-To-Cell Signaling and Interaction	activation	2.17E-03	CD22, SOCS2, CD274	BCL2L1, CD63, ITGA3, ITGB3, MAP2K3, PPARG, , STC1, TNFSF4, TP53, VIPR2	13
Cellular Growth and Proliferation	proliferation	2.92E-03	CD22, CD274, PTX3, SOCS2	AKAP13, ANGPTL4, BCL2L1, CTH, DECR1, DKK1, EDNRA, ID2, ITGA3, ITGB3, LRIG1, PDE2A, PPARG, PRDM1, RAC2, RALB, ROMO1, SERPINA1, SFRP1, STC1, TFPI2, TGFBI, TNFSF4, TP53, ZMIZ1	29
Gene Expression	transcription	1.04E-02	DLX2, SOCS2	AKAP5, AKAP13, ATXN1, BCL2L1, BHLHE41, DKK1, FSTL3, HIVEP3, ID2, ITGB3, MAP2K3, NR2F2, PLK2, PPARG, PRDM1, SFRP1,TCEA2, TCEAL1, TP53, ZMIZ1	22